DNA and RNA Telomeric G-Quadruplexes: What Topology Features Can be Inferred from Ion Mobility Mass Spectrometry?

Valentina D'Atri‡, Valérie Gabelica*

University of Bordeaux, INSERM and CNRS, ARNA Laboratory, IECB site, 2 rue Robert Escarpit, 33600 Pessac, France.

* Corresponding author: v.gabelica@iecb.u-bordeaux.fr

‡ Current address: *School of Pharmaceutical Sciences, University of Geneva, University of Lausanne, CMU, Rue Michel Servet 1, 1211, Geneva 4, Switzerland*

SUPPORTING INFORMATION

Table of Contents

Table S1: Instrument tuning parameters.

Parameter	8-repeat RNAs	others
Ion Polarity	Negative	Negative
Source: gas temperature	200 °C	200 °C
Source: drying gas	3.0 L/min	3.0 L/min
Source: nebulizer pressure	13 psig	14 psig
Source: capillary	3500 V	3500 V
Optics 1: Fragmentor	-350 V or -600 V	-350 V or -600 V
IM front funnel: high pressure funnel delta	-150 V	-150 V
IM front funnel: high pressure funnel RF	**-200 V**	-120 V
IM front funnel: trap funnel delta	**-140 V**	-150 V
IM front funnel: trap funnel RF	**-210 V**	-200 V
IM front funnel: trap funnel exit	-10 V	-10 V
IM trap: trap entrance grid low	**-105 V**	-102 V
IM trap : trap entrance grid delta	**-5 V**	-6 V
IM trap: trap entrance	-101 V	-101 V
IM trap: trap exit	-99 V	-99 V
IM trap: trap exit grid 1 low	**-97 V**	-95 V
IM trap: trap exit grid 1 delta	-6 V	-6 V
IM trap: trap exit grid 2 low	**-96 V**	-94 V
IM trap: trap exit grid 2 delta	**-7 V**	-10 V
Acquisition: Trap fill time	600 µs	600 µs
Acquisition: Trap release time	100 µs	100 µs
IM drift tube: Drift tube exit	-210 V	-210 V
IM rear funnel: Rear funnel entrance	-200 V	-200 V
IM rear funnel: Rear funnel RF	-200 V	-200 V
IM rear funnel: Rear Funnel Exit	-35 V	-35 V
IM rear funnel: IM Hex Entrance	-32 V	-32 V
IM rear funnel: IM Hex Delta	-3 V	-3 V
Optics 1: Oct Entrance Lens	-27 V	-27 V
Optics 1: Oct 1 DC	-25 V	-25 V
Optics 1: Lens 1	-23 V	-23 V
Optics 1: Lens 2	-10.5 V	-10.5 V
Quad: Quad DC	-21 V	-21 V
Quad: PostFilter DC	-21 V	-21 V
Cell: gas flow	20 psi	20 psi
Cell: Cell Entrance	-20 V	-20 V
Cell: Hex DC	-20 V	-20 V
Cell: Hex Delta	3 V	3 V
Cell: Hex2 DC	-14.6 V	-14.6 V
Cell: Hex2 DV	1.5 V	1.5 V
Optics 2: Hex3 DC	-12.9 V	-12.9 V
Extractor: Ion Focus	-10 V	-10 V

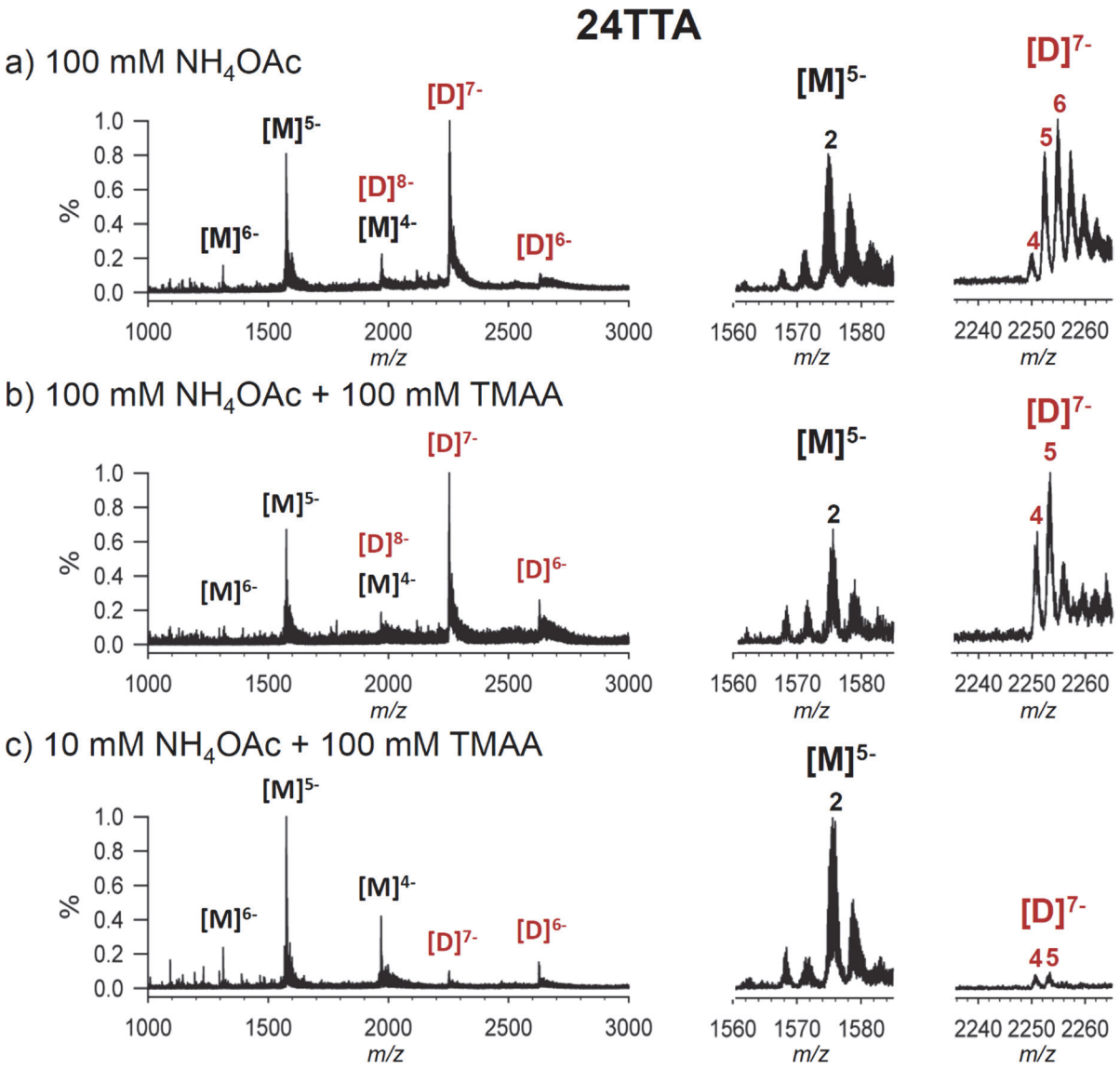

Figure S1: Effect of the cation size on multimer formation.
ESI-MS spectra of sequence 24TTA in three different conditions: a) 100 mM NH_4OAc, b) 100 mM NH_4OAc and 100 mM TMAA, and c) 10 mM NH_4OAc and 10 mM TMAA.

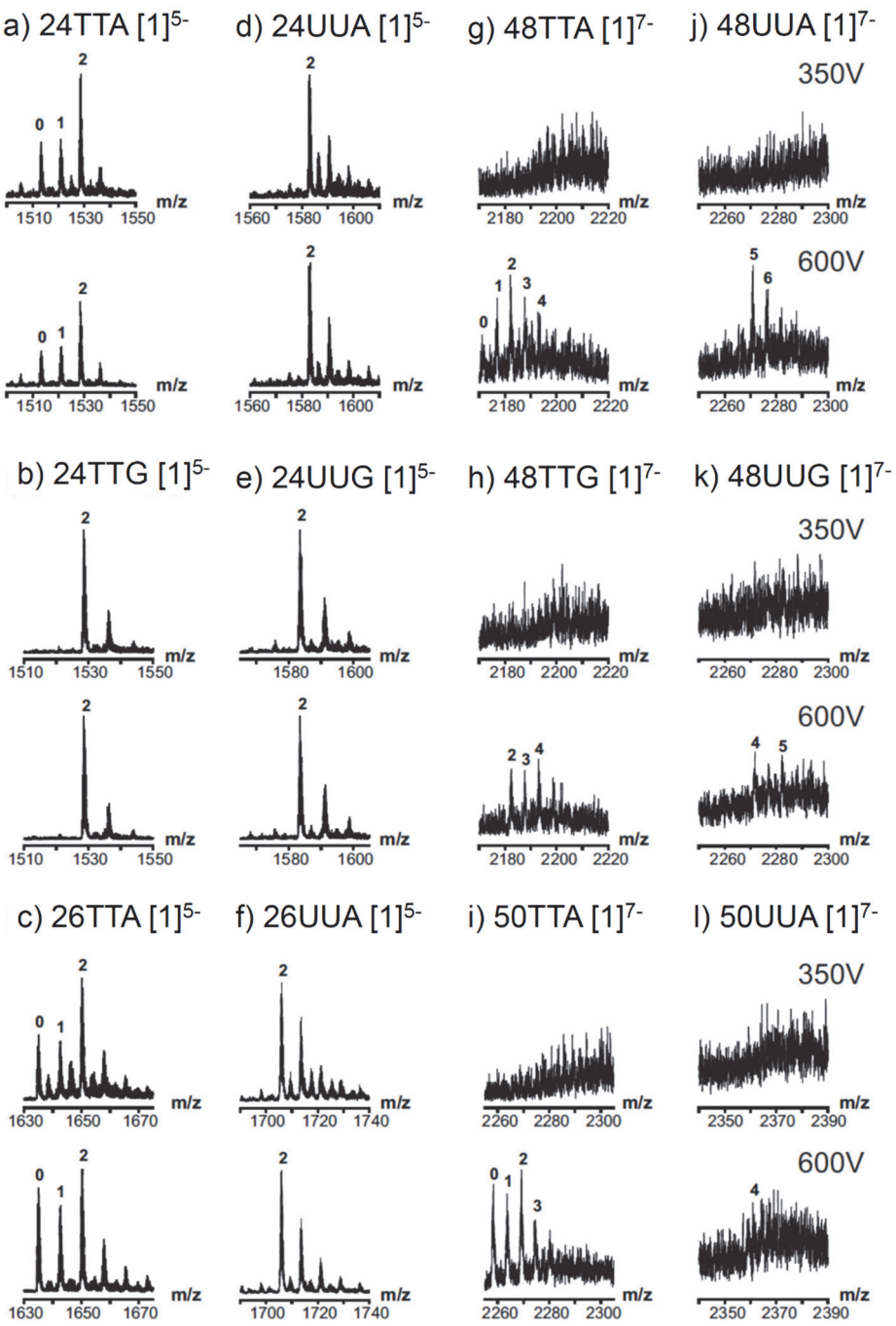

Figure S2: K^+ ion binding measured by ESI-MS.
Zoom of the ESI-IM-MS spectra (fragmentor: 350 V on top and 600 V on bottom) showing the distribution of the number of potassium ions preserved in the intramolecular structures of (a) 24TTA, (b) 24TTG, (c) 26TTA, (d) 24UUA, (e) 24UUG, (f) 26UUA, (g) 48TTA, (h) 48TTG, (i) 50TTA, (j) 48UUA, (k) 48UUG, and (l) 50UUA. Annotation $[n]^{z-}$ stands for species of molecularity *n* at the *z*- charge state, and the number of potassium ions are indicated on each peak.

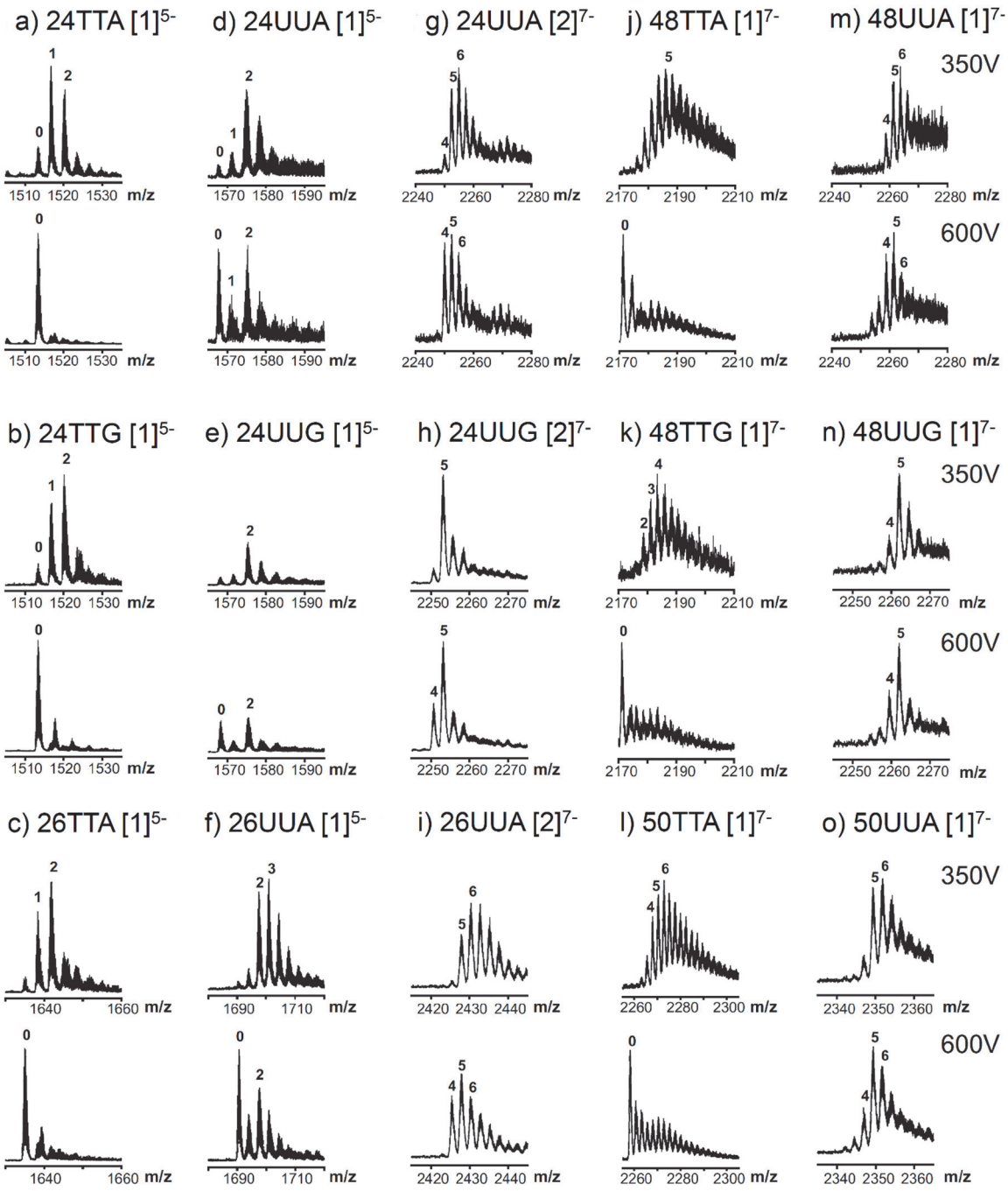

Figure S3: NH_4^+ ion binding measured by ESI-MS.
Zoom of the ESI-IM-MS spectra (fragmentor: 350 V on top and 600 V on bottom) showing the distribution of the number of ammonium ions preserved in the structure of (a) 24TTA, (b) 24TTG, (c) 26TTA, (d) intramolecular 24UUA, (e) intramolecular 24UUG, (f) intramolecular 26UUA, (g) bimolecular 24UUA, (h) bimolecular 24UUG, (i) bimolecular 26UUA, (j) 48TTA, (k) 48TTG, (l) 50TTA, (m) 48UUA, (n) 48UUG, and (o) 50UUA. Annotation $[n]^{z-}$ stands for species of molecularity *n* at the *z*- charge state, and the number of ammonium ions are indicated on each peak.

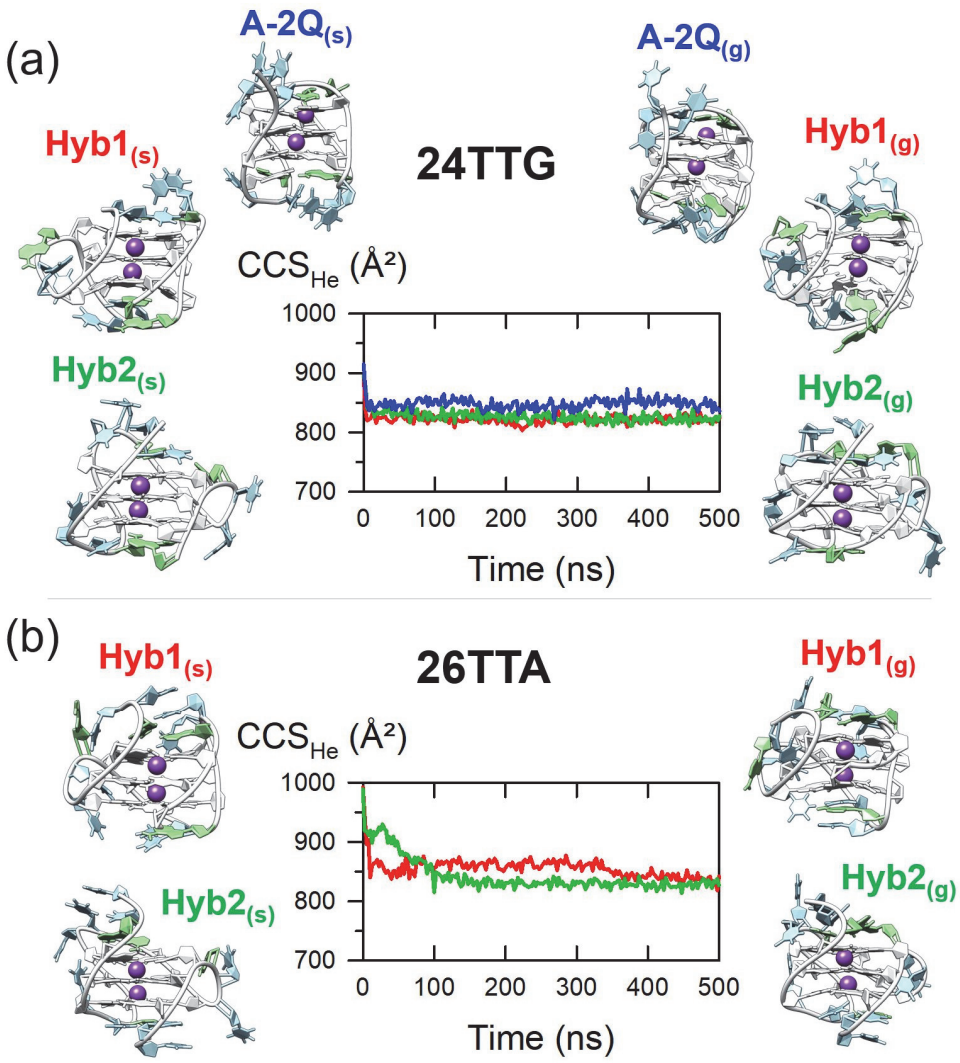

Figure S4: Structural rearrangements upon gas-phase MD for a) 24TTG and b) 26TTA. Evolution of the collision cross section as a function of gas-phase molecular dynamics. Structures on the left are solution models extracted from solution MD, which served as starting points for gas-phase force field MD. Structures on the right are gas-phase structures extracted after 200 ns of gas-phase force field MD.

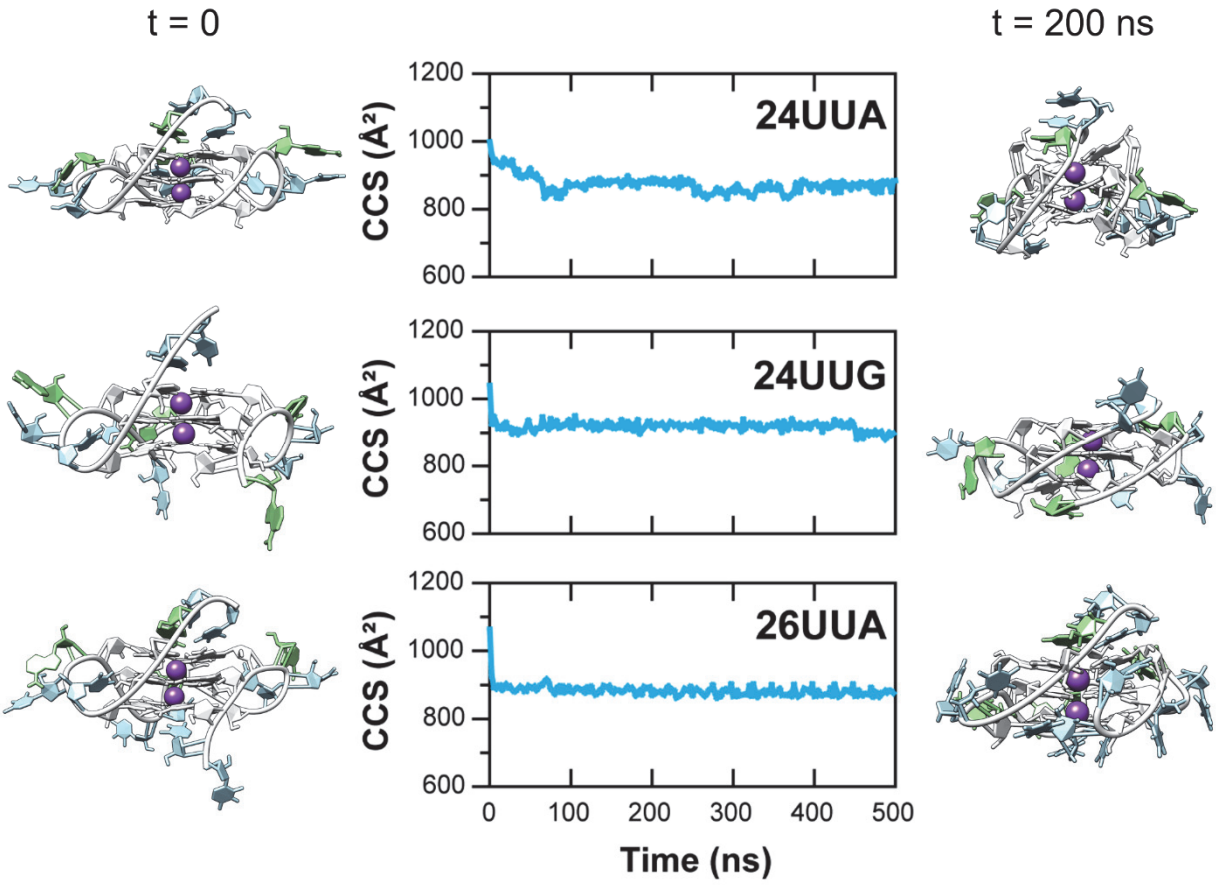

Figure S5: Evolution of 4-repeat RNA parallel structural models upon gas-phase MD. Evolution of the collision cross section as a function of gas-phase molecular dynamics. Structures on the left are solution models extracted from solution MD, which served as starting points for gas-phase force field MD. Structures on the right are gas-phase structures extracted after 200 ns of gas-phase force field MD.

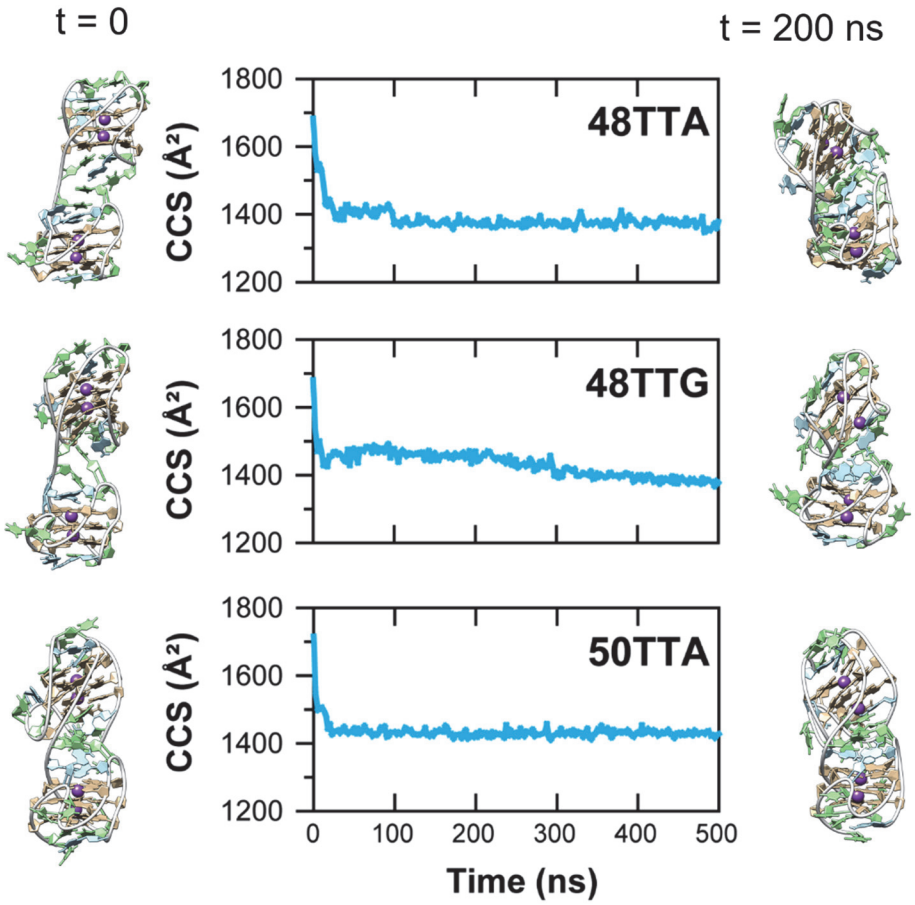

Figure S6: Evolution of 8-repeat DNA beads-on-string structural models upon gas-phase MD.

Evolution of the collision cross section as a function of gas-phase molecular dynamics. Structures on the left are solution models extracted from solution MD, which served as starting points for gas-phase force field MD. Structures on the right are gas-phase structures extracted after 200 ns of gas-phase force field MD.

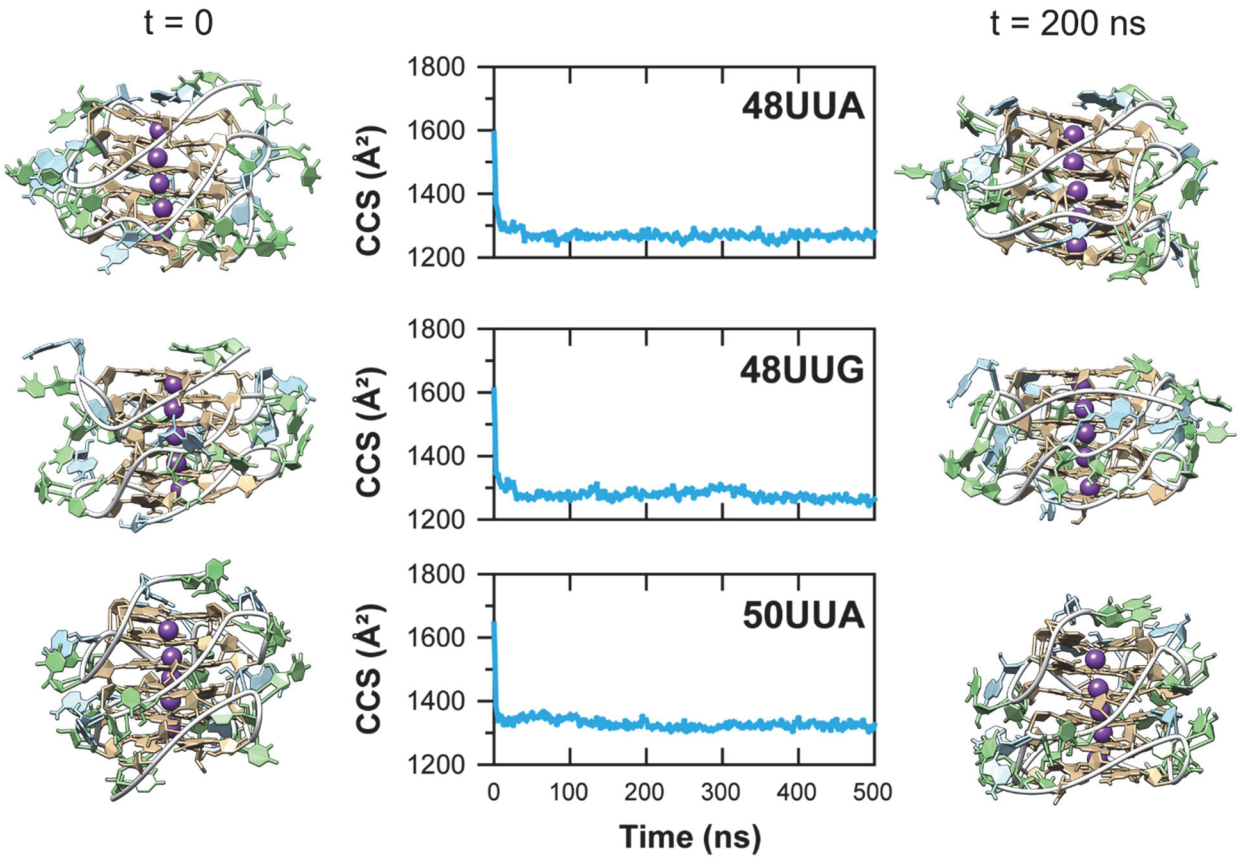

Figure S7: Evolution of 8-repeat RNA parallel structural models upon gas-phase MD. Evolution of the collision cross section as a function of gas-phase molecular dynamics. Structures on the left are solution models extracted from solution MD, which served as starting points for gas-phase force field MD. Structures on the right are gas-phase structures extracted after 200 ns of gas-phase force field MD.

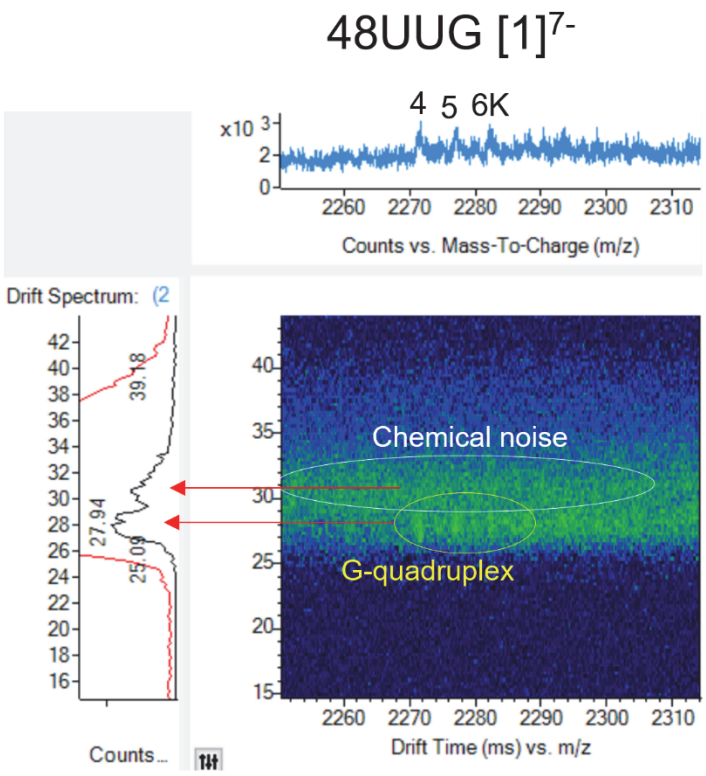

Figure S8: Proof that the hump at long arrival times of 8-repeat RNA $[1]^{7-}$ is chemical noise. The figures shows the 2D projection map of the mass spectrum (horizontal axis) and drift time spectrum (vertical axis). The chemical noise shows up at all *m/z* values, whereas the structure-specific mobility peaks show only at specific *m/z* ratios corresponding to 4, 5 or 6 K^+ adducts.

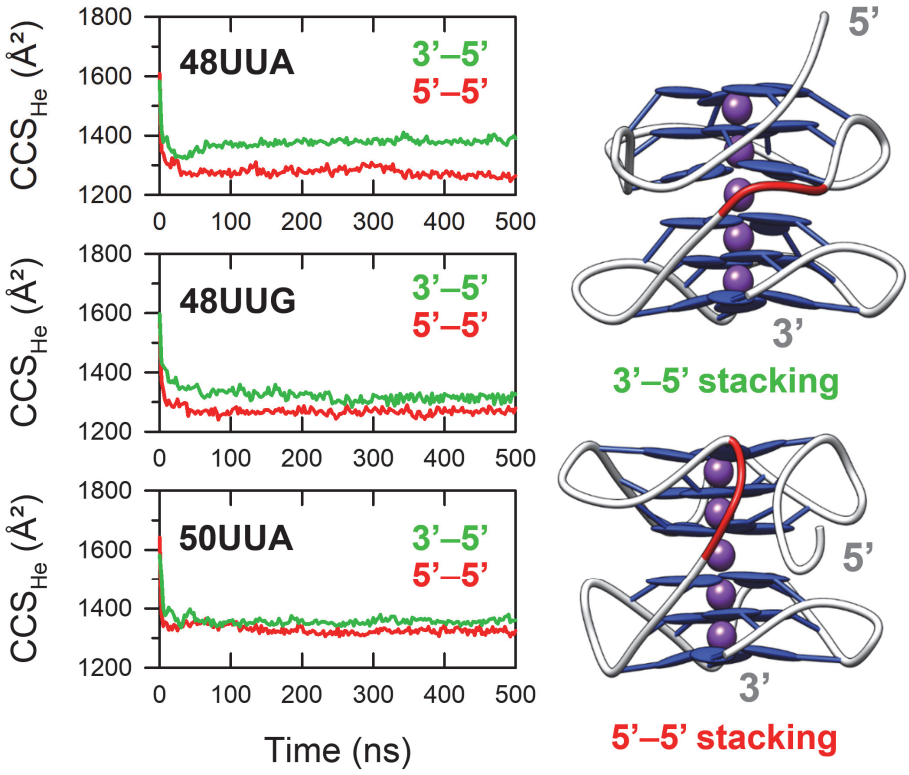

Figure S9: 8-repeat RNA parallel structural models: comparison between 3'–5' stacking and 5'–5' stacking.
Left: evolution of the collision cross section as a function of gas-phase molecular dynamics. Structures on the right illustrate where the linking loop (red) was placed.